JPE 17-2-17

https://doi.org/10.6113/JPE.2017.17.2.490
ISSN(Print): 1598-2092 / ISSN(Online): 2093-4718

Stability Analysis of FCHEV Energy System Using Frequency Decoupling Control Method

Peng Dai*, Weinan Sun†, Houqing Xie*, Yan Lv*, and Zhonghui Han*

*,†School of Electrical and Power Engineering, China University of Mining and Technology, Xuzhou, China

Abstract

Fuel cell (FC) is a promising power supply in electric vehicles (EV); however, it has poor dynamic performance and short service life. To address these shortcomings, a super capacitor (SC) is adopted as an auxiliary power supply. In this study, the frequency decoupling control method is used in electric vehicle energy system. High-frequency and low-frequency demand power is provided by SC and FC, respectively, which makes full use of two power supplies. Simultaneously, the energy system still has rapidity and reliability. The distributed power system (DPS) of EV requires DC–DC converters to achieve the desired voltage. The stability of cascaded converters must be assessed. Impedance-based methods are effective in the stability analysis of DPS. In this study, closed-loop impedances of interleaved half-bridge DC–DC converter and phase-shifted full-bridge DC–DC converter based on the frequency decoupling control method are derived. The closed-loop impedance of an inverter for permanent magnet synchronous motor based on space vector modulation control method is also derived. An improved Middlebrook criterion is used to assess and adjust the stability of the energy system. A theoretical analysis and simulation test are provided to demonstrate the feasibility of the energy management system and the control method.

Key words: DC bus, DC–DC converter, Frequency decoupling control, Impedance, Permanent magnet synchronous motor

I. INTRODUCTION

The increasingly serious environmental pollution and energy depletion problems causes the urgency for new energy. Fuel cell (FC) is a promising distributed power supply; it has the advantages of high efficiency and low pollution, but has the disadvantages of poor dynamic performance and short service life [1]-[3]. Super capacitor (SC) offers an alternative approach to manage power flows within various electrical system applications, such as uninterruptible and portable power supplies, renewable energy generation systems, and hybrid electric vehicle (HEV). SC is characterized by high efficiency, fast charging and discharging, extended cycle life, relatively high-specific power, and wide operating temperature range; thus, SCs are suitable in compensating the disadvantages of FCs [4]-[6]. This study presents a hybrid power supply system with PEMFC as the main power supply and an SC pack as the auxiliary power supply.

Manuscript received Sep. 1, 2016; accepted Dec. 30, 2016
Recommended for publication by Associate Editor Jonghoon Kim.
†Corresponding Author: 276412965@qq.com
Tel: +86-0516-83885667, Fax: +86-0516-83885667, China University of Mining and Technology
*School of Electrical and Power Engineering, China University of Mining and Technology

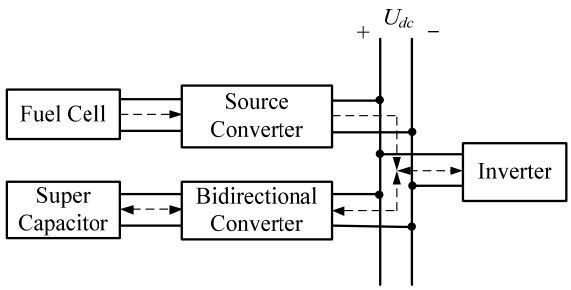

Fig. 1. Structure and energy flows of fuel cell hybrid electric vehicle (FCHEV) energy system.

The FC–SC hybrid power system is shown in Fig. 1, which contains an FC pack, an SC pack, a source converter, a bidirectional converter, and an inverter load. In this system, energy is delivered from the FC to the DC bus. The inverter transports energy in both directions. Meanwhile, the bidirectional converter compensates for the shortcomings of the FC due to poor dynamics and failure to recycle energy.

The load of the electric vechicle (EV) is variable and random in response to unsteady traffic, including frequent acceleration, deceleration, uphill, or downhill runs. Therefore, the energy management strategy must add a regulation mechanism to ensure power sharing strategy for a significant

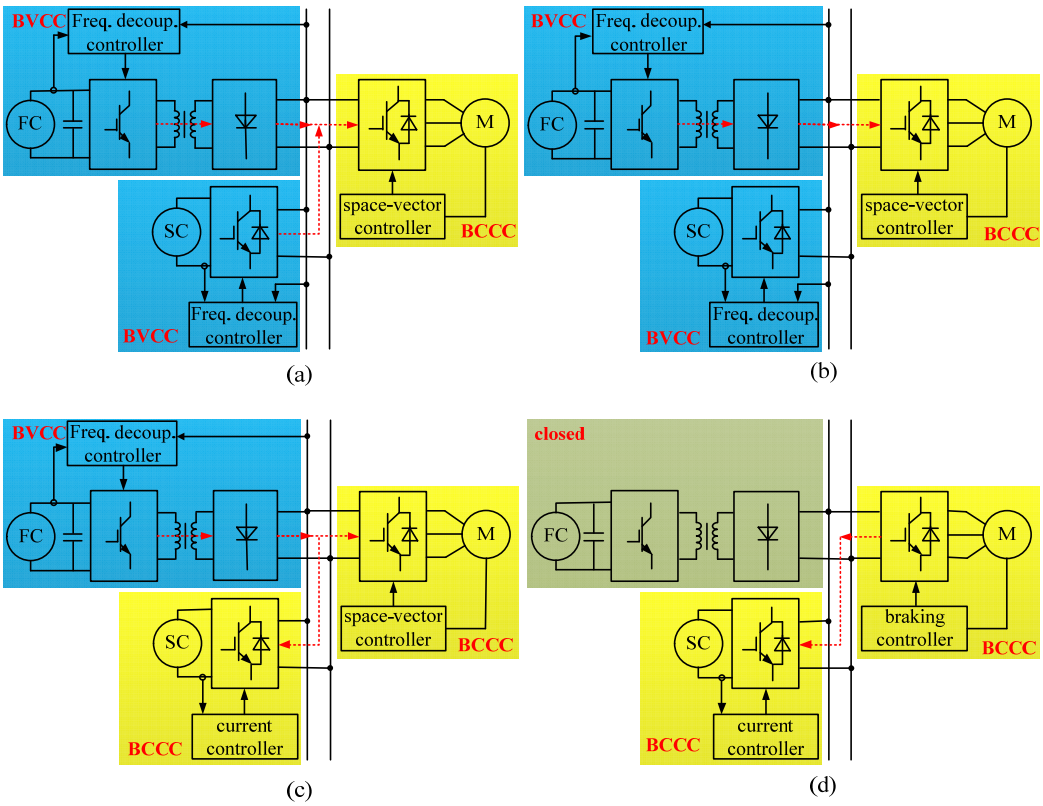

Fig. 2. Structure, control method, and energy flows of FC–SC hybrid driving system in different operating modes.

reduction in the variations of FC current, which is beneficial to its service life. This strategy is equivalent to requiring the reduction of the high-frequency variations of the FC current [7]-[9]. In this study, a high-pass filter (HPF) and a low-pass filter (LPF) are used in the power system to realize the frequency decoupling control method.

DC–DC converters with feedback control have been widely used in applications, such as space stations, aircraft, shipboards, communication systems, renewable energy systems, and hybrid vehicles. These applications require tight output regulation, fast response, and high power quality. However, this feedback control makes the input power instantaneously constant; thus, the converter acts as a constant power load with negative impedance characteristic. This characteristic may destabilize the operation of the entire system. The problem on the interaction of the cascaded electric system is well known, and numerous works have already been published to explain this phenomenon [10]-[16]. The cascaded system may become unstable because of the interaction between the subsystems, although each subsystem may operate properly as an individual system [17]. The impedance-based method is effective for stability analysis of the cascaded distributed power system.

This paper is organized as follows. The energy management strategy and stability analysis method are reviewed in Section II. Derivations of two converters and inverter for permanent magnet synchronous motor (PMSM) impedance are presented in Section III. Stability analysis, adjustment, and system test are discussed in Section IV. Conclusions are presented in Section V.

II. Review of Energy Management Strategy and Stability Analysis Method

A. Review of Energy Management Strategy in HEV Energy System

At present, multisource supply systems are a subject of extended research investigation using advanced control methods, as well as the electrical vehicular applications. In the last decade, different energy management strategies for FCHEV power systems have been reported [18]-[23]. In [18] and [19], the system is appropriately controlled by a rule-based strategy; however, the performances of the energy system depend on previous experiences. In [22] and [23], the system is appropriately controlled by a model predictive control strategy and neural networks strategy, respectively. However, these strategies are extremely complex and require large computation. An energy system based on a classical PI controller [20] has been proposed recently, which is easily tuned online for better tracking and does not require any expert knowledge. In this study, the PI controller and frequency decoupling methods are adopted to ensure that the main source provides low-frequency demand power, whereas the other sources deal with high-frequency demand power

that can protect the FC and ensure rapidity of the system simultaneously.

Frequency decoupling control method was first used in wind and photovoltaic generator system. Classical wind or solar energy conversion systems are usually passive generators. The generated power does not depend on the load requirement but entirely on the fluctuant power condition [30]–[31]. The frequency decoupling control method has been adopted to achieve maximum efficiency and stable output simultaneously. In the EV power systems, the main source of output power must be stable, while the demand power of load is fluctuant, which is similar to the generation systems. This control method is also applicable to the EV power system. Some articles on frequency decoupling control method in FCHEV energy system have been published in [7]–[9], [32]–[34].

The FC–SC hybrid energy system has four possible operating modes, which are shown in Fig. 2. A brief introduction is provided in the following description.

Operating mode I [Fig. 2(a)]: A sudden increase in the demand energy of the motor, such as starting and accelerating decreases the DC bus voltage, which affects the stability of both the driving and energy systems. The SC and FC must provide more energy to compensate for the change. In this mode, both the source and bidirectional converter are controlled by the frequency decoupling control method. Closed-loop PI regulators are adopted to ensure the rapidity and stability of the DC bus voltage.

Operating mode II [Fig. 2(b)]: When the demand energy of the motor is nearly constant, the demand power of the load is entirely provided by the FC, which can be realized automatically by the frequency decoupling control method. *Mode* II can be regarded as the special conditions of *Mode* I; however, *Mode* II is more likely to occur in actual conditions.

Operating mode III [Fig. 2(c)]: When the voltage of SC is lower than the given value, *Mode* III should appear to ensure that the SC has sufficient energy for potential *Mode* I. In this mode, the source converter is controlled by the frequency decoupling method, and the bidirectional converter is controlled by constant current charging. This mode should occur at a smoothly running period because it cannot deal with the changing load in time but can guarantee the safety of the FC.

Operating mode IV [Fig. 2(d)]: The motor can assist a mechanical brake when the EV needs to stop. Simultaneously, regenerative energy and energy restored in the DC bus can be recycled to the SC. In this mode, the DC bus voltage does not need to maintain the rated value. The regenerative energy will not be restored if the SC is already fully charged.

B. Introduction of Stability Analysis Method on EV Energy System

Although many energy management methods have been proposed and tested, the stability of the power system under these strategies did not attract much attention. Attention has been provided to high-level performances, such as energy assumption, SOC of power source, and vehicle acceleration performance. Conversely, low-level performances, such as output current and DC bus voltage, which are based on topology structure of the energy system, have not been analyzed and adjusted. In this study, the stability of the low-level performance is analyzed.

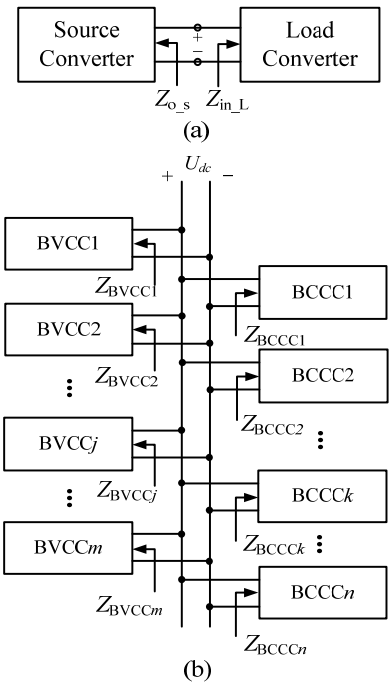

Fig. 3. (a) Typical structure of cascaded electric system. (b) General form of the multi-input multi-output (MIMO) converter system.

Given that the small signal model can be achieved, as shown in Fig. 4, the Nyquist criterion or other stability criterion based on frequency characteristics can be adopted to assess the stability of the subsystems individually. However, these criteria cannot easily assess the stability of the entire system. Therefore, the impedance-based method, which is effective for the stability analysis of complex systems, is adopted in this study.

The impedance-based method is effective for assessing the stability of the cascaded electric system. For the typical cascaded system in Fig. 3(a), the ratio of the output impedance of the source converter Z_{o_s} and the input impedance of the load converter Z_{in_L} can equivalently represent the loop gain of the cascaded system. Moreover, both the source and load converters are individually stable, and the amplitude of Z_{o_s} is less than Z_{in_L} in the entire frequency range; thus, the stability of the cascaded system is guaranteed. This criterion is proposed by Middlebrook [24]. Although this criterion is effective in assessing the stability of the cascaded electric system, the application of the criterion

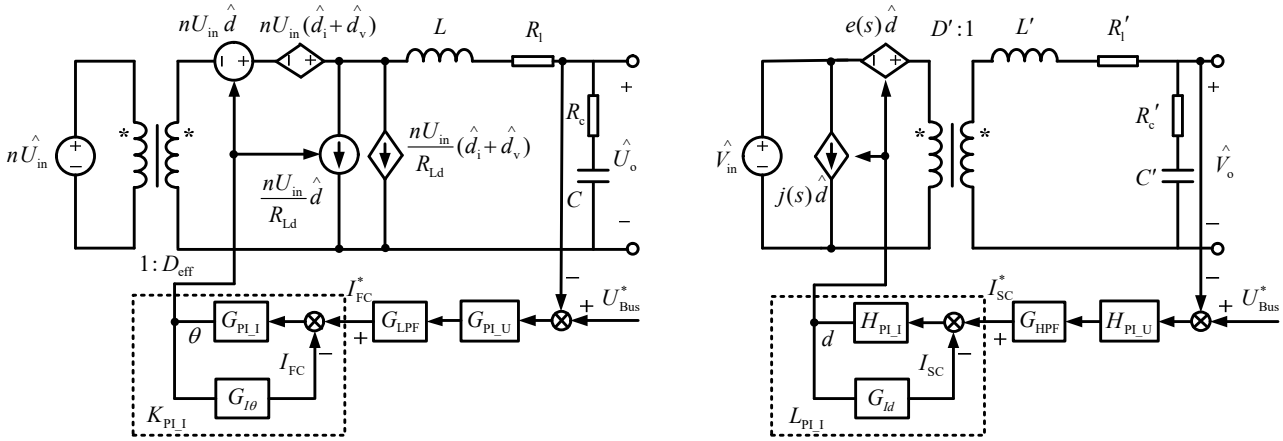

Fig. 4. Closed-loop small-signal models of DC–DC converter: (a) phase-shifted full-bridge (PSFB) converter. (b) Boost converter.

in MIMO converter system is no longer useful. The energy system in this study is a multi-input single-output converter system, which is a special form of the MIMO converter system. Therefore, the classical Middlebrook criterion is no longer applicable.

Recently, it has been found that any converter in a DC distributed power system (DPS) is either a bus voltage control converter (BVCC) or a bus current control converter (BCCC). BVCC refers to a converter that controls or affects its bus-side port voltage. BCCC refers to a converter that controls or affects its bus-side port current. Based on BVCC and BCCC, the general form of a MIMO converter system is obtained, as shown in Fig. 3(b). m (m≥1) BVCCs and n (n≥1) BCCCs are connected in parallel. Then, the following equation is obtained:

$$\begin{aligned} Z_{\mathrm{BVCC}} &= \left(\sum_{j=1} 1/Z_{\mathrm{BVCC}j}\right)^{-1} \\ Z_{\mathrm{BCCC}} &= \left(\sum_{i=1} 1/Z_{\mathrm{BCCC}i}\right)^{-1} \end{aligned}. \tag{1}$$

If the converters are all individually stable, and the amplitude of Z_{BCCC} is greater than Z_{BVCC} in the entire frequency range, the stability of the cascaded system is guaranteed. On the basis of the criterion in [25], the stability analysis of the FC–SC hybrid power system can be assessed and adjusted. In *Operating modes* I and II, the source converter and bidirectional converter are controlled by the high- and low-frequency components of the voltage difference, respectively. Thus, these converters are both BVCC. In *Operating mode* III, the source converter is controlled by the low-frequency component of voltage difference, and the bidirectional converter is controlled by the current difference. Thus, the source converter is BVCC, whereas the bidirectional converter is BCCC. In *Operating mode* IV, the two converters are both BCCC. Given that the stability of the subsystems in this power system have already been studied and accepted, this study focuses on the stability of the interaction in the entire system. Therefore, the analytical expression of the input impedance of the inverter for the motor drive system and the output impedance of the two converters must be established, which is presented in Section III.

III. Derivation of Converters and Inverter for PMSM Impedances

The stability criterion for DC DPS requires the closed-loop impedance of converters. The closed-loop small-signal models of the source and bidirectional converters with frequency decoupling control are shown in Fig. 4. These models use an LPF and HPF to limit the variations of FC current, and compensate for the delay of FC. The filters used in the control method may greatly influence the closed-loop impedance. Thus, in this section, converter impedances and load under the frequency decoupling control method are derived.

A. Derivation of Source Converter Closed-loop Impedance with LPF

The PSFB PWM converter is adopted as the source converter in this study. According to previous studies in [26], a small-signal model includes both the duty cycle loss of the secondary side of the transformer and the equivalent series resistance of the inductor and capacitor, as shown in Fig. 4(a). Then, the transfer function of the output filter is derived as

$$H(s)=\frac{1+s\cdot R_c\cdot C}{1+s\cdot C\cdot(R_c+R_l)+s^2\cdot L\cdot C}, \tag{2}$$

where L and C are output filter inductance and capacitance, respectively. R_l and R_c are the equivalent series resistances of inductor and capacitor, correspondingly.

The input impedance of the output filter is expressed as:

$$Z_{1i}=\frac{1+s\cdot R_c\cdot C}{H(s)\cdot s\cdot C}. \tag{3}$$

The output impedance of the output filter is expressed as follows:

$$Z_{1o} = H(s)\cdot(R_{\mathrm{l}} + s\cdot L)\,. \tag{4}$$

The simplified control-to-output transfer function is

$$G_{vd} = \frac{n\cdot V_{\mathrm{i}}\cdot\omega_0^2}{s^2 + 2\omega_0\cdot\xi\cdot s + \omega_0^2}, \tag{5}$$

where n is the transformer ratio, and V_{i} is the input voltage. $\omega_0 = \frac{1}{\sqrt{L\cdot C}}$, and ξ is the damping of the second-order denominator.

$$\xi = \frac{R_{\mathrm{d}}}{2}\sqrt{\frac{C}{L}}, \tag{6}$$

where $R_{\mathrm{d}}=4n^2L_{\mathrm{r}}f_{\mathrm{s}}$, L_{r} is the resonant inductance, and f_{s} is the switching frequency. The open-loop output impedance of the PSFB power stage is

$$Z_{1o\_o} = Z_{1o} + \frac{H^2(s)}{1/Z_{1i}(s) + 1/R_{\mathrm{d}}}\,. \tag{7}$$

According to the control block diagram shown in Fig. 4(a) and the definition of the closed-loop output impedance, the closed-loop output impedance can be obtained. Given that the current loop is set to rapidly track the given front value, the entire current loop can be treated as a proportion component $K_{\mathrm{PI\_I}}$ by reducing the time constant of the current loop. The transfer function of an LPF is defined as G_{LPF}. The closed-loop output impedance of PSFB DC–DC converter is

$$Z_{1o\_cl} = \frac{Z_{1o\_o}}{1 + G_{\mathrm{PI\_U}}\cdot G_{\mathrm{LPF}}\cdot K_{\mathrm{PI\_I}}\cdot G_{vd}}\,. \tag{8}$$

B. Derivation of Bidirectional Converter Closed-loop Impedance with HPF

This paper adopts the interleaved half-bridge DC–DC converter as the bidirectional converter. The two-phase converters share the same control and main circuit (half-switching period delay of interleaving can be ignored in the derivation); thus, the two phases of the parallel interleaved DC–DC converter are relatively independent and completely symmetrical. Therefore, the output impedance of the parallel interleaved boost converter is equal to half the value of that in the boost circuit. Based on this analysis, the output impedance of the interleaved converter is obtained from the boost converter.

Similar to the derivation of the source converter, the open-loop output impedance of the bidirectional converter can be achieved by the small-signal analysis. The small-signal model of boost circuit is shown in Fig. 4(b).

According to the small-signal model, the open-loop output impedance of the boost circuit in the CCM mode can be obtained as follows:

$$Z_{2o\_o} = \frac{s^2\cdot L'\cdot C'\cdot R_{\mathrm{c}}' + s(L' + R_{\mathrm{c}}'\cdot R_{\mathrm{l}}'\cdot C') + R_{\mathrm{l}}'}{s^2\cdot C'\cdot L' + s(R_{\mathrm{c}}'\cdot C'\cdot D'^2 + R_{\mathrm{l}}'\cdot C') + D'^2}, \tag{9}$$

where L' and C' are output filter inductance and capacitance, and R_{l}' and R_{c}' are equivalent series resistances of the inductor and capacitor, respectively. $e(s) = U_o(1 - s\cdot L/R\cdot D'^2)$, $j(s) = U_o/D'^2R$.

The simplified control-to-output transfer function is

$$G_{ud} = \frac{V_{in}}{L'\cdot C'\cdot s^2 + D'^2}\,. \tag{10}$$

Similar to the derivation of the source converter, the entire current loop is treated as a proportion component $L_{\mathrm{PI\_I}}$. According to the control block diagram shown in Fig. 4(b) and the definition of the closed-loop output impedance, the closed-loop impedance of the boost converter in the CCM mode is

$$Z_2 = \frac{Z_{2o\_o}}{1 + H_{\mathrm{PI\_U}}\cdot G_{\mathrm{HPF}}\cdot L_{\mathrm{PI\_I}}\cdot G_{ud}}\,. \tag{11}$$

Finally, the output impedance of the parallel interleaved boost converter in CCM mode is expressed as:

$$Z_{2o\_cl} = \frac{Z_{2o\_o}}{2(1 + H_{\mathrm{PI\_U}}\cdot G_{\mathrm{HPF}}\cdot L_{\mathrm{PI\_I}}\cdot G_{ud})}\,. \tag{12}$$

C. Closed-loop Impedance of the Inverter for PMSM with Id=0 Control Method

The classical space vector control method is adopted in this paper. The average model and small-signal analysis can be used to derive the input impedance of the system [27]–[29]. With the use of Park transformation, the voltage, current, and electromechanical characteristic equations can be modeled in the rotating d–q domain, as shown as follows:

$$\begin{aligned} V_{\mathrm{d}} &= (R_{\mathrm{d}} + L_{\mathrm{d}}\cdot s)I_{\mathrm{d}} - L_{\mathrm{q}}\cdot I_{\mathrm{q}}\cdot P\cdot\omega \\ V_{\mathrm{q}} &= (R_{\mathrm{q}} + L_{\mathrm{q}}\cdot s)I_{\mathrm{q}} + (\psi + L_{\mathrm{d}}\cdot I_{\mathrm{d}})\cdot P\cdot\omega \\ T_{\mathrm{e}} &= \frac{3}{2}P\cdot[\psi\cdot I_{\mathrm{q}} + I_{\mathrm{d}}\cdot I_{\mathrm{q}}(L_{\mathrm{d}} - L_{\mathrm{q}})] \\ \omega &= \frac{1}{J\cdot s}(T_{\mathrm{e}} - T_{\mathrm{L}}) \end{aligned}, \tag{13}$$

where V_{d} and V_{q} are equivalent voltages of the motor in the d–q domain; I_{d} and I_{q} are equivalent currents of the motor in the d–q domain; R_{d}, R_{q}, L_{d}, and L_{q} are equivalent resistances and inductances of the motor in the d–q domain; P is the number of the pole pairs; ω is motor speed; Ψ is the rotor flux linkage; J is the motor inertia; and T_{e} and T_L are electromagnetic torque and load torque, respectively.

The following equation is defined:

$$\begin{aligned} D(s) &= R_{\mathrm{d}} + L_{\mathrm{d}}\cdot s \\ Q(s) &= R_{\mathrm{q}} + L_{\mathrm{q}}\cdot s \\ M(s) &= P^2\cdot L_{\mathrm{d}}\cdot L_{\mathrm{q}}\cdot\omega_0^2 + D(s)\cdot Q(s) \end{aligned}\,. \tag{14}$$

The small-signal model of the d–q current is shown in Fig. 5. If the inverter does not experience power loss, the power balance equation is

$$V_{\mathrm{dc}}I_{\mathrm{dc}} = \frac{3}{2}(V_{\mathrm{d}}I_{\mathrm{d}} + V_{\mathrm{q}}I_{\mathrm{q}})\,, \tag{15}$$

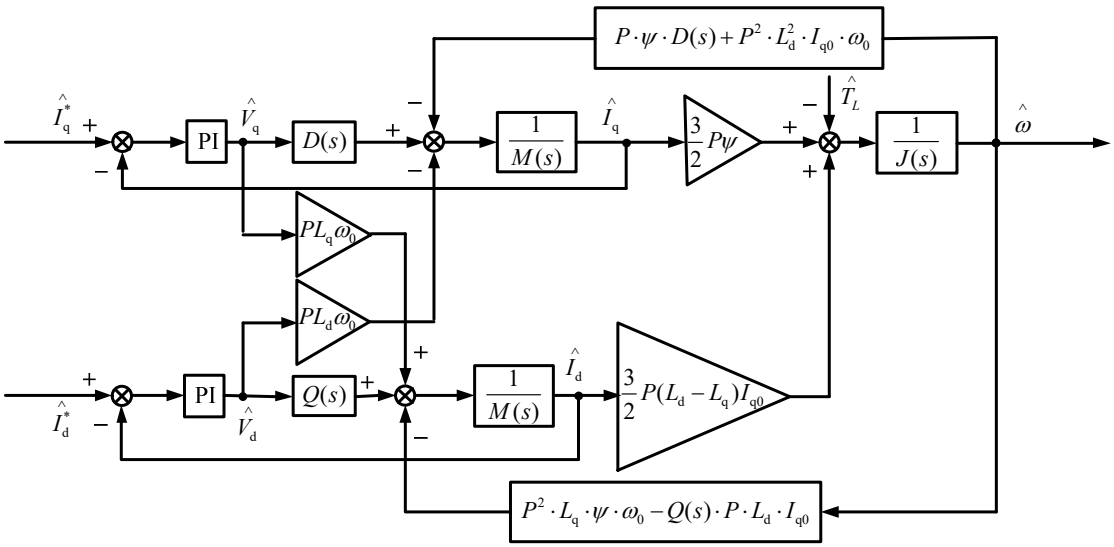

Fig. 5. Small-signal model of the d–q current loops in the inverter for PMSM.

where V_{dc} is the voltage of the DC bus, and I_{dc} is the current of the DC bus, which flows into the inverter. Then, the small signal relation between DC bus variables and d–q domain variables can be obtained.

$$\hat{V}_{dc} I_{dc0} + \hat{I}_{dc} V_{dc0} = \frac{3}{2}(V_{d0}\hat{I}_d + V_{q0}\hat{I}_d + I_{q0}\hat{V}_q + I_{d0}\hat{V}_d) \quad (16)$$

Variables with the subscript 0 denote the steady-state value of the variables. To simplify the complexity of the derivation, the speed loop regulator is neglected because it is remarkably slower than the current loop. The current loop model in Fig. 5 and Equation (16) is used to eliminate $\hat{I}_d, \hat{I}_q, \hat{V}_d, \hat{V}_q$., and $\hat{T}_L$, and $\hat{I}_q^*$ are assumed to be zero. The small-signal input impedance can be derived as:

$$Z_{3i\_cl} = \frac{\hat{V}_{dc}}{\hat{I}_{dc}} = \frac{V_{dc0}}{\frac{3}{2}V_{dc0}(H_1 + H_2\cdot V_{q0}) - I_{dc0}}, \quad (17)$$

where

$$H_1(s) = \frac{-L_q\cdot P^2\cdot\omega_0^2\cdot I_{q0}^2(L_d - L_q)}{D(s)+G_{PI}(s)}$$
$$H_2(s) = \frac{V_{q0} + I_{q0}[Q(s) + {3P^2\cdot\psi^2}/{2J\cdot s}]}{G_{PI}(s)+Q(s)} \quad (18)$$

When the closed-loop impedances of the converters and inverter have been derived, system stability of the system can be analyzed using the impedance-based method. Analysis and test are shown in the following section.

IV. Stability Adjustment And Test of The Energy System

A. Analysis and Adjustment of the Energy System Stability

Fig. 2 shows the topology of the FCHEV energy system.

TABLE I
MOTOR SPECIFICATIONS

Parameters	Values
Rated speed	2000 rpm
Rated torque	10.5 N·m
Rated current	6.8 A
Number of pole-pairs	3
Stator resistance	0.5 Ω
Q-axis inductance	8.5 mH
D-axis inductance	4.5 mH
Inertia constant	3.1e−3 kg·m^2
Switching frequency	5 kHz

TABLE II
POWER SUPPLIES SPECIFICATIONS

Parameters	Values
FC voltage at 0 A	42 V
FC voltage at 1 A	35 V
FC nominal point	(52 A, 24.23 V)
FC maximum point	(100 A, 20 V)
FC dynamics preset	No
SC capacitance	1 F
SC rated voltage	80 V
SC initial voltage	70 V
SC surge voltage	100 V

In this system, the source converter is a PSFB PWM DC–DC converter, whereas the bidirectional converter is an interleaved half-bridge DC–DC converter. A PEMFC–1.26 kW–24 VDC hydrogen FC model is adopted. The capacitance

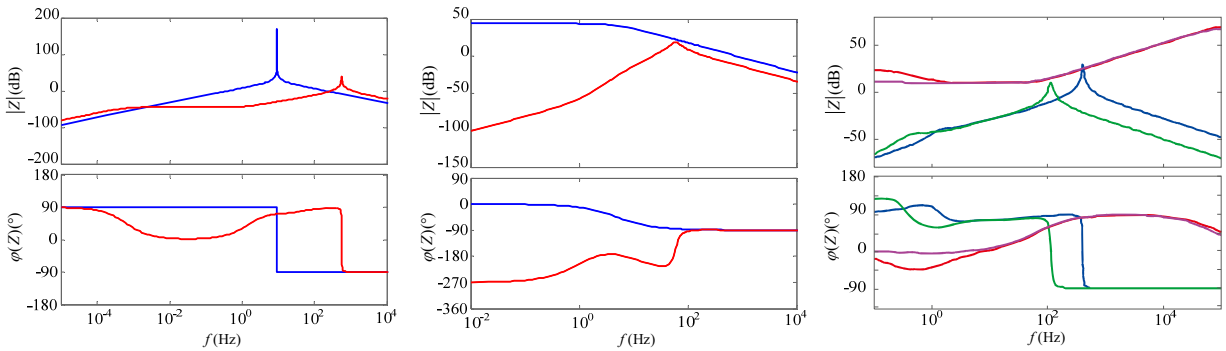

Fig. 6. Bode plots of each part of the energy system impedances: (a) Open- and closed-loop impedances of the source converter. (b) Open- and closed-loop impedances of the bidirectional converter. (c) Z_{BCCC} and Z_{BVCC} of the energy system at different loads and different DC bus capacitances.

value and rated voltage of the SC are 1 F and 80 V, respectively. The parameters of PMSM and the two power supplies are shown in Tables I and II, respectively

Given that the main purpose of this study is to verify the stability of the energy system using the frequency decoupling control method, the stability analysis and simulation were only conducted in *Operating modes* I and II. Therefore, the voltage of SC is assumed not to be extremely low in the entire operating process.

The impedances of the two converters and the motor inverter are shown in Fig. 6. The open- and closed-loop impedances of the source converter are shown in Fig. 6(a) in blue and red curves, respectively. The open-and closed-loop impedances of the bidirectional converter are shown in Fig. 6(b) in blue and red curves, respectively. These two figures show that the open and closed-loop impedances of the converter are different. Z_{BCCC} and Z_{BVCC} of the energy system at different loads and different DC bus capacitances are shown in Fig. 6(c). The red curve represents the impedance when the load is T_L=1 N·m, ω=150rad/s. The violet curve represents the impedance when the load is T_L=5N·m, ω=150rad/s. The figure shows that the Bode plots of the inverter for motor impedance are similar despite the different loads, especially at the middle and high frequencies. According to the basic theory in [25], the Z_{BVCC} and Z_{BCCC} of the system can be obtained using Equation (19). The Bode plots are shown in Fig. 6(c). Blue and green curves represent Z_{BVCC}; red and violet curves represent Z_{BCCC}.

$$Z_{BVCC}=\left(\sum_{j=1}\frac{1}{Z_{BVCCj}}\right)^{-1}=\left(\frac{1}{Z_{1o\_cl}}+\frac{1}{Z_{2o\_cl}}\right)^{-1} \quad (19)$$

$$Z_{BCCC}=\left(\sum_{i=1}\frac{1}{Z_{BCCCi}}\right)^{-1}=Z_{3i\_cl}$$

Fig. 6(c) shows the intersection between $|Z_{BVCC}|$ and $|Z_{BCCC}|$ at approximately 400 Hz when C_{bus}=800 μF (the capacitance of the DC bus). In this case, the FC–SC hybrid energy system will be unstable and oscillate. Although many existing solutions can eliminate the intersection, only the most practical method in reducing $|Z_{BVCC}|$ is utilized. C_{bus} can be adjusted to realize this target. If the value of C_{bus} is adjusted from 800 μF to 2000 μF, the condition wherein the amplitude of the improved Z_{BVCC} is lower than that of the Z_{BCCC} in the entire frequency range can be obtained, as shown in Fig. 6(c) (green curve represents Z_{BVCC} when C_{bus}=2000 μF). According to the impedance-based stability analysis theory, the system is stable in this case.

The stability adjustment results of the system, shown in Fig. 7, verify the conclusion above, where the waveforms of U_{dc}, I_{FC}, and I_{SC} are used to show the oscillations. Fig. 7(a) illustrates that although the power system is stable before t=0.6 s (T_L=1 N·m, ω=150 rad/s, the SC does not have an output in the stable situation), oscillations in these waveforms appear after t=0.6 s (T_L suddenly changes to 5 N·m at 0.6 s); thus, the system is unstable. By adjusting C_{bus} from 800 μF to 2000 μF, the voltage and currents, shown in Fig. 7(b), are well damped, and the oscillations in the waveforms disappear; thus, the system has better dynamic stability properties in this case. The dynamic of the motor shown in Fig. 9 is acceptable. Thus, 2000 μF is an acceptable adjustment for this application.

B. Simulation Test of the System

When the stability has been assessed and adjusted, the test of the energy system based on the frequency decoupling control method can be performed. Simulation has been done in this study, and the simulation conditions are as follows:

- The total simulation time is set to 2 s.
- When $0\le t<0.6$ s, set T_L=1 N·m, and the demand speed of the motor is set to 150 rad/s (approximately 1433 rpm).
- When $0.6\ s\le t<1.5$ s, set T_L=5 N·m with the demand speed unchanged.
- When t=1.5 s, the motor brakes at once.

The output waveforms of the SC and FC in the test are shown in Fig. 8. Red and blue curves represent the SC and FC, respectively. When $0\le t\le t_1$, FC and SC output high power together, until the DC bus voltage reaches the given value. When $t_1<t<t_2$, the demand power is approximately maintained constant; thus, the FC provides the power alone. When $t=t_2$, a sudden increase in T_L occurs, and the demand power suddenly

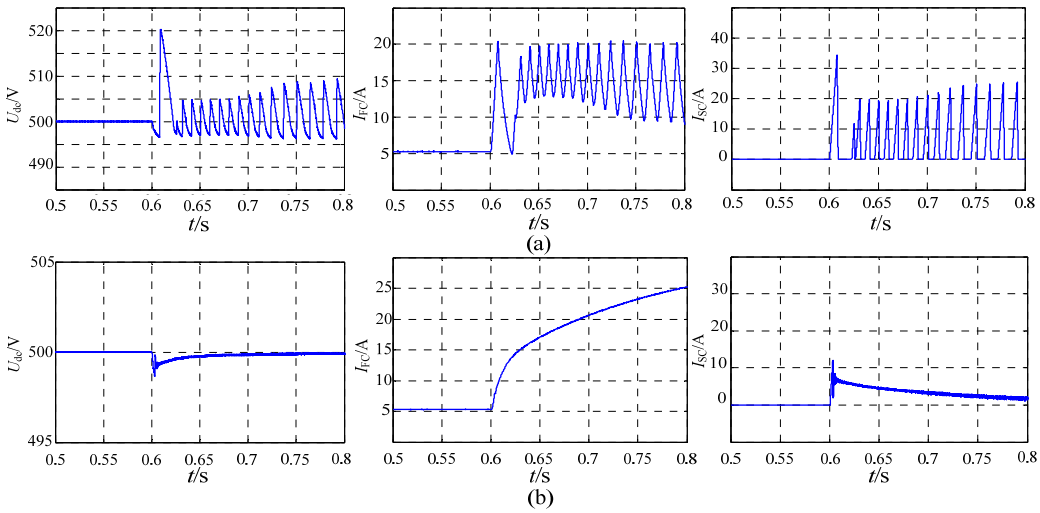

Fig. 7. DC bus voltage (U_{dc}) waveform, FC, and SC current waveforms (I_{FC}, I_{SC}) using frequency decoupling control method. (a) When C_{bus} is equal to 800 μF.(b) When C_{bus} is adjusted to 2000 μF.

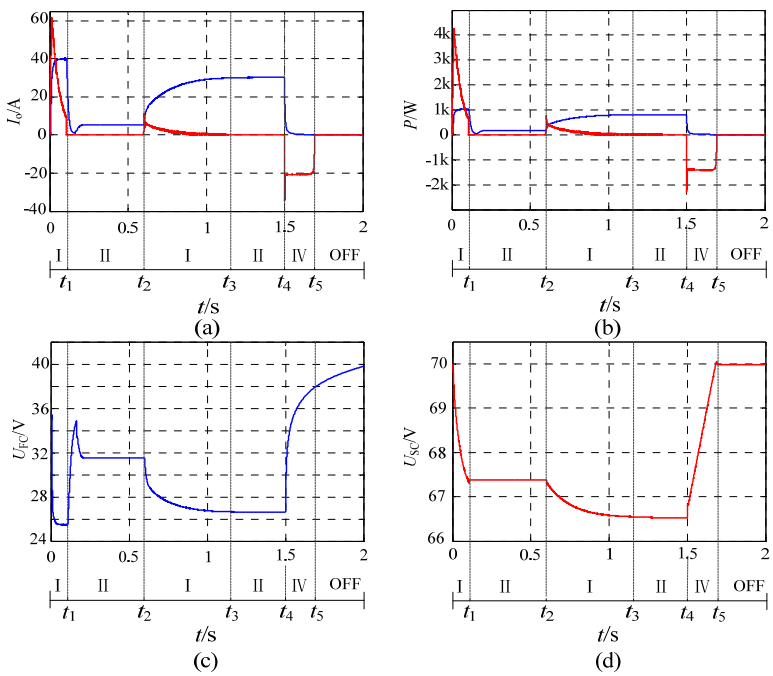

Fig. 8. FC and SC current waveforms using frequency decoupling control method. FC: blue, SC: red.

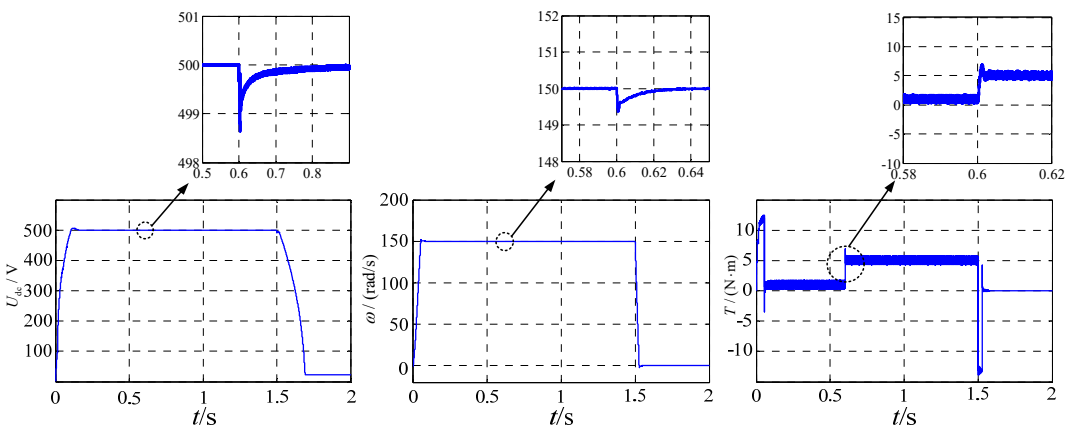

Fig. 9. DC bus voltage (U_{dc}), motor speed (ω), and motor electromagnetic torque (T_e) waveforms.

increases; thus, the FC and SC provide low- and high-frequency components of the demand power, respectively.

In Fig. 8(a) and 8(c), the change rates of the FC current and voltage are evidently slower after t=0.6 s. FC delay time is approximately 0.5 s, which is beneficial to maintain the service life. Fig. 9 shows that the DC bus and the motor are still rapid and stable during the delay time. After the delay time, the FC output current can track the given precisely. Figs. 8(a), 8(b), and 8(d) show the SC output current, power, and voltage, respectively. The maximum output power of the SC reaches 4 times the maximum output power of the FC in this test, which makes full use of the large discharging current of the SC. When the demand power is approximately constant, SC output will be automatically adjusted to 0. When $t=t_4$, the motor brakes. The energy in the driving system can be recycled, which is shown in the SC voltage in Fig. 8(d). The high efficiency of FCs, together with the energy recovery function of the SC can greatly increase the energy system efficiency.

Fig. 9 shows the operation of the DC bus and the motor. The driving system can run smoothly with the front energy system in the entire test. The waveforms of the motor can be stable by adjusting the parameters of the PI regulator. Given that the motor control unit is not the focus in this study, the motor is only used to test the rapidity and stability of the energy system in this study, which is set to a harder test than the actual situation.

In summary, the FC–SC hybrid power system can improve the exploitation of the FC, and maintain the rapidity and stability of the energy system and the driving system simultaneously using the frequency decoupling control method. The low-frequency demand power is provided by the FC, which leads to slow current and voltage changes. The SC plays an important role due to its advantages of fast discharging rate and ability to recycle energy. With the stable and rapid energy system, the performance of the motor load is acceptable. The test result agrees with the stability analysis result described in this article.

V. CONCLUSIONS

This paper introduced an improved Middlebrook criterion to the FCHEV energy system. The dynamic stability of the energy system was assessed and adjusted using frequency decoupling control method. Closed-loop impedances of two converters and the inverter for PMSM load were derived. HPF and LPF were used to separate different frequency components of demand power. The multisource supply system can improve FC exploitation, and maintain the rapidity and stability of the energy system and the driving system simultaneously using the frequency decoupling control method. Given that this study focuses on theoretical analysis, further research should be made in experimental and actual road condition tests.

ACKNOWLEDGMENT

This work was supported in part by the Qinglan Innovation Project of Jiangsu Province in China under Grant 04150020, and in part by the Research Innovation Program for College Graduates of Jiangsu Province in China under Grant SJLX16_0630.

REFERENCES

[1] C. C. Chan, "The state of the art of electric, hybrid, and fuel cell vehicles," *Proceedings of the IEEE*, Vol. 95, No. 4, pp. 704-718, Apr. 2007.

[2] K. Sedghisigarchi and A. Feliachi, "Impact of fuel cells on load-frequency control in power distribution systems," *IEEE Trans. Energy Convers.*, Vol. 21, No. 1, pp. 250-256, Mar. 2006.

[3] J. S. Lai and D. J. Nelson, "Energy management power converters in hybrid electric and fuel cell vehicles," *Proceedings of the IEEE*, Vol. 95, No. 4, pp. 766-777, Apr. 2007.

[4] A. F. Burke, "Batteries and ultracapacitors for electric, hybrid, and fuel cell vehicles," *Proceedings of the IEEE*, Vol. 95, No. 4, pp. 806-820, Apr. 2007.

[5] P. Thounthong, S. Rael, and B. Davat, "Utilizing fuel cell and supercapacitors for automotive hybrid electrical system," in *20th Annual IEEE Applied Power Electronics Conference and Exposition (APEC)*, pp. 90-96, Mar. 2005.

[6] H. Rahimi-Eichi, U. Ojha, F. Baronti, and M.-Y. Chow, "Battery management system: an overview of its application in the smart grid and electric vehicles," *IEEE Ind. Electron. Mag.*, Vol. 7, No. 2, pp. 4-16, Jun. 2013.

[7] A. Florescu, A. I. Bratcu, I. Munteanu, A. Rumeau, and S. Bacha, "LQG optimal control applied to on-board energy management system of all-electric vehicles," *IEEE Trans. Control Syst. Technol.*, Vol. 23, No. 4, pp. 1427-1439, Jul. 2015.

[8] H. Alloui, K. Marouani, M. Becherif, M. N. Sid, and M. E. H. Benbouzid, "A control strategy scheme for fuel cell-vehicle based on frequency decoupling," in *International Conference on Green Energy*, pp. 170-175, Mar. 2014.

[9] X. Zhang and C. Mi, *Vehicle power management: modeling, control and optimization*, Springer, Vol. 14, No. 2, pp. 91-118, Jan. 2011.

[10] X. Zhang, Q. C. Zhong, and W. L. Ming., "Stabilization of cascaded DC/DC converters via adaptive series-virtual-impedance control of the load converter," *IEEE Trans. Power Electron.*, Vol. 31, No. 9, pp. 6057-6063, Sep. 2016.

[11] X. Feng, J. Liu, and F. C. Lee, "Impedance specifications for stable DC distributed power systems," *IEEE Trans. Power Electron.*, Vol. 17, No. 2, pp. 157-162, Mar. 2002.

[12] A. Emadi, "Modelling of power electronic loads in AC distribution systems using the generalized state space averaging method," *IEEE Trans. Ind. Electron.*, Vol. 51, No. 5, pp. 992-1000, Oct. 2004.

[13] X. Xiong, C. K. Tse, and X. Ruan, "Bifurcation analysis of standalone photovoltaic-battery hybrid power system," *IEEE Trans. Circuits Syst. I, Reg. Papers*, Vol. 60, No. 5, pp. 1354-1365, May 2013.

[14] A. Khaligh, "Realization of parasitics in stability of DC–DC converters loaded by constant power loads in advanced multiconverter automotive systems," *IEEE Trans. Ind.*

Electron., Vol. 55, No. 6, pp. 2295-2305, Jun. 2008.
[15] A. M. Rahimi and A. Emadi, "Active damping in DC/DC power electronic converters: a novel method to overcome the problems of constant power loads," *IEEE Trans. Ind. Electron.*, Vol. 56, No. 5, pp. 1428-1439, May 2009.
[16] M. Huang, S. C. Wong, C. K. Tse, and X. Ruan, "Catastrophic bifurcation in three-phase voltage-source converters," *IEEE Trans. Circuits Syst. I, Reg. Papers*, Vol. 60, No. 4, pp.1062-1071, Apr. 2013.
[17] X. Zhang, X. Ruan, H. Kim, and C. K. Tse, "Adaptive active capacitor converter for improving the stability of cascaded DC power supply system," *IEEE Trans. Power Electron.*, Vol. 28, No. 4, pp. 1807-1816, Apr. 2013.
[18] P. Garcia, L. M. Fernandez, C. A. Garcia, and F. Jurado, "Energy management system of fuel-cell-battery hybrid tramway," *IEEE Trans. Ind. Electron.*, Vol. 57, No. 12, pp. 4013-4023, Dec. 2010.
[19] S. Caux, W. Hankache, M. Fadel, and D. Hissel, "On-line fuzzy energy management for hybrid fuel cell systems," *International Journal of Hydrogen Energy*, Vol. 35, No. 5, pp. 2134-2143, Mar. 2010.
[20] Z. Amjadi and S. S. Williamson, "Power-electronics-based solutions for plug-in hybrid electric vehicle energy storage and management systems," *IEEE Trans. Ind. Electron.*, Vol. 57, No. 2, pp. 608-616, Feb. 2010.
[21] B. Vural, A. R. Boynuegri, I. Nakir, O. Erdinc, A. Balikci, M. Uzunoglu, H. Gorgun, and S. Dusmez, "Fuel cell and ultra-capacitor hybridization: A prototype test bench based analysis of different energy management strategies for vehicular applications," *International Journal of Hydrogen Energy*, Vol. 35, No. 20, pp. 11161-11171, Oct. 2010.
[22] W. Greenwell and A. Vahidi, "Predictive control of voltage and current in a fuel cell–ultracapacitor hybrid," *IEEE Trans. Ind. Electron.,* Vol. 57, No. 6, pp. 1954-1963, Jun. 2010.
[23] J. Moreno, M. E. Ortuzar, and J. W. Dixon, "Energy management system for a hybrid electric vehicle, using ultracapacitors and neural networks," *IEEE Trans. Ind. Electron.*, Vol. 53, No. 2, pp. 614-623, Apr. 2006.
[24] R. D. Middlebrook, "Input filter considerations in design and application of switching regulators," in *Proceeding of the IEEE IAS*, pp. 366-382, 1976.
[25] X. Zhang, X. Ruan, and C. K. Tse, "Impedance-based local stability criterion for DC distributed power systems," *IEEE Trans. Circuits Syst. I, Reg. Papers*, Vol. 62, No. 3, pp. 916-925, Mar. 2015.
[26] V. Vlatković, J. A. Sabaté, R. B. Ridley, F. C. Lee, and B. H. Cho, "Small-signal analysis of the phase-shifted PWM converter," *IEEE Trans. Power Electron.*, Vol. 7, No. 1, pp. 128-135, Jan. 1992.
[27] X. Liu and A. J. Forsyth, "Active stabilization of a PMSM drive system for aerospace applications," in *IEEE Power Electronics Specialists Conference (PESC)*, pp. 283-289, Jun. 2008.
[28] X. Liu, A. J. Forsyth, and A. M. Cross, "Negative input resistance compensator for a constant power load," *IEEE Trans. Ind. Electron.*, Vol. 54, No. 6, pp. 3188-3196, Dec. 2007.
[29] S. D. Sudhoff, K. A. Corzine, S. F. Glover, H. J. Hegner, and H. N. Robey, "DC link stabilized field oriented control of electric propulsion systems," *IEEE Trans. Energy Convers.*, Vol. 13, No. 1, pp. 27-33, Mar. 1998.
[30] Z. Tao and B Francois, "Energy management and power control of a hybrid active wind generator for distributed power generation and grid integration," *IEEE Trans. Ind. Electron.*, Vol. 58, No. 1, pp. 95-104, Jan. 2011.
[31] Q. Jiang, Y. Gong, and H. Wang, "A battery energy storage system dual-layer control strategy for mitigating wind farm fluctuations," *IEEE Trans. Power Syst.*, Vol. 28, No. 3, pp. 3263-3273, Aug. 2013.
[32] A. Tani, M. B. Camara, and B. Dakyo, "Energy management based on frequency approach for hybrid electric vehicle applications: fuel-cell/lithium-battery and ultra- capacitors," *IEEE Trans. Veh. Technol.*, Vol. 61, No. 8, pp. 3375-3386, Oct. 2012.
[33] A. Tani, M. B. Camara, B. Dakyo, and Y. Azzouz, "DC/DC and DC/AC converters control for hybrid electric vehicles energy management-ultracapacitors and fuel cell," *IEEE Trans. Ind. Informat.*, Vol. 9, No. 2, pp. 686-696, May 2013.
[34] S. N. Motapon, L. A. Dessaint, and K. Al-Haddad, "A comparative study of energy management schemes for a fuel-cell hybrid emergency power system of more electric aircraft," *IEEE Trans. Ind. Electron.*, Vol. 61, No. 3, pp. 1320-1334, Mar 2014.

Peng Dai received his B.S. degree from the School of Electrical Engineering, Anhui University of Science and Technology, Huainan, China in 1994. He received his M.S. and Ph.D. degrees from the School of Information and Electrical Engineering, China University of Mining and Technology, Xuzhou, China in 1998 and 2004, respectively. Since 1998, he has been with the School of Information and Electrical Engineering, China University of Mining and Technology, where he is currently a professor. His current research interests include power electronics, motor drives, and renewable power generation.

Weinan Sun received his B.S. degree in Electrical Engineering from China University of Mining and Technology, Xuzhou, China in 2015. Since 2015, he has been working toward his M.S. degree in China University of Mining and Technology. His current research interests include power electronics, DC–DC converters, and AC motor control.

Houqing Xie received his B.S. degree in Electrical Engineering from China University of Mining and Technology, Xuzhou, China in 2012. He joined Sungrow Power Supply, Hefei, China in 2012, where he devoted himself to developing the automatic test system of a photovoltaic inverter. Since 2015, he has been working toward his M.S. degree in China University of Mining and Technology. His research interests include electric motor drivers and PMSM control.

Yan Lv received his B.S. degree in Electrical Engineering from China University of Mining and Technology, Xuzhou, China in 2014. Since 2014, he has been working toward his M.S. degree in China University of Mining and Technology. His current research interests include power electronics and AC synchronous motor control.

Zhonghui Han received his B.S. degree in Electrical Engineering from China University of Mining and Technology, Xuzhou, China in 2016. Since 2016, he has been working toward his M.S. degree in China University of Mining and Technology. His current research interests include electric motor drivers and PMSM control.